nature portfolio

https://doi.org/10.1038/s41558-022-01430-5

## Supplementary information

# Vertically migrating phytoplankton fuel high oceanic primary production

In the format provided by the authors and unedited

# Supporting Online Material
# for "Vertically migrating phytoplankton fuel high oceanic primary production"

Kai Wirtz, S. Lan Smith, Moritz Mathis, Jan Taucher

## S1 Model skill: vertical, temporal, and lateral variability in NPP

Most Net Primary Production (NPP) occurs near the surface: at each of the four stations, more than 75% of depth integrated NPP ($NPP_\Sigma$) derives from the upper 20m (at marine station K2) to 60m (at stations BATS, HOT), well above both the chemocline and the subsurface chlorophyll maximum (SCM). Active migrators, which form the SCM in our simulations, directly contribute a minor fraction of total $NPP_\Sigma$, which is negligible at the sites K2 and S1 with their shallow chemocline (Fig. S2). However, biological N-pumping by migrators can on average explain an additional 25% of the N-demand for production by the non-migrating autotrophic community, ranging from 15% at K2 to 36% at BATS[1].

Our account of primary production by vertical migrators and indirect contributions through their nutrient pumping enables a consistent parameterization of the processes sustaining production, especially for the (dominant) contribution by non-migrating phytoplankton (Fig. S2). As a result, the model demonstrates a high skill of reproducing NPP profiles, with explained variance ($r^2$) of log-transformed vertically resolved NPP of 0.53 at BATS ($n$=3040), 0.71 at HOT ($n$=2107), 0.51 at S1 ($n$=110), and 0.73 at K2 ($n$=128). The good agreement is apparent in the direct comparison of model results with observed multi-scale variability at HOT and BATS (Fig. 2). Also simulated $NPP_\Sigma$ at HOT and BATS fits the long-term average of the data and amplitude of temporal fluctuations including single events. Error statistics of log-transformed $NPP_\Sigma$ at both sites show a low $r^2$ of 0.06 at HOT and 0.05 at BATS, respectively, together with a low bias of 0.0 and 0.03 and a small root-mean-squared error (RMSE) of 0.14 and 0.26. Model performance decreases when phytoplankton vertical migration (PVM) is switched off (HOT bias/RMSE 0.04/0.14, BATS: 0.09/0.32). For the period 2005–2010, for which data from both time-series were compared to state-of-the-art satellite-based models[2], the RMSE further reduces to 0.11 (HOT) and 0.22 (BATS), thus lying at

the lower end of reported error values, which indicates relatively high model skill.

This is remarkable given the many simplifications in our modeling approach, such as assuming steady-state conditions over many days to weeks of each migration cycle. That particular assumption may however explain the more homogeneous vertical distribution of simulated NPP in Fig. 2 compared to the data at both stations. Notwithstanding, the non-uniform decline of NPP with increasing depth is very well reproduced, as is evident from the good agreement between climatological profiles of model results and observations in Extended Data Fig. 1. This includes station K2, for which our parametrization assumes co-limitation by iron. For comparison, the model of Li et al.[3] with otherwise high skill in reproducing physical and BGC states in the northwestern Pacific, largely underestimated NPP near the surface (0–50m) at K2. Overall, our mechanistic model appears realistically sensitive to changes in ambient conditions and captures vertical gradients in production to an unprecedented degree.

Lateral variability in time-integrated $NPP_{\Sigma}$ was assessed using both model set-ups (station based and global). In the application to the four oceanic sites, simulated $NPP_{\Sigma}$ agree very well with observed rates (Extended Data Fig. 2), as can be expected from the comparison of spatially and temporally resolved values. Also in our global set-up using different forcing data, $NPP_{\Sigma}$ correlates with previous observations from cruises, as compiled by Saba et al[4], Chavez et al[5] and Buitenhuis et al[6] (Extended Data Fig. 2). However, the global model systematically underestimates observed primary production rates with calculated $NPP_{\Sigma}$ at BATS 40% lower than in the time-series application, likely because the boundary conditions used in the global application were less accurate (e.g., climatologies of remotely sensed surface CHL or of interpolated CARS2009 data for $NO_3$) compared to the *in situ* data used as boundary input in the time-series application (e.g., up-to-date surface CHL and $NO_3$ profiles for estimating chemocline depth). We decided against recalibrating the model for this current global application to corroborate the conservative nature of our NPP estimates thus aiming for a low estimate of global NPP within the possible model range, and also to facilitate later integration of more precise global boundary data.

In the current parametrization, the Indian Ocean, North and South Equatorial Current, and Central Atlantic Ocean including the Caribbean Sea almost entirely feature annual rates above 700 mg-$Cm^{-2}d^{-1}$. Very low values of $NPP_{\Sigma}$ are instead estimated for the North Pacific or upwelling

regions mostly because of high residual nitrate in these areas (Fig. S4). While assumed limitation by, e.g., iron and concomitant reduction in $NPP_{\Sigma}$ seems realistic for the North Pacific and its prevalent high-nitrate low-chlorophyll state[7], it can be regarded as a model artifact for the Namibian and Peruvian upwelling systems.

## S2 Multiple evidence for slow vertical migration

The potential relevance of a non-physical transport mechanism such as biological pumping is further supported by stable isotope observations from the Sargasso Sea, which suggest that eukaryotic autotrophs in the nutrient-poor euphotic zone obtain their nitrogen mainly from deep water nitrate[8], rather than from the mostly refractory dissolved organic nitrogen[9], and that this nitrate assimilation in the euphotic zone roughly matches the vertical export flux[10].

A few taxa such as mat forming diatoms, dinoflagellates, and some cyanobacteria reach swimming or floating velocities of several tens of metres per day[11–14], much faster than bulk phytoplankton species that display velocities of around 0.4–4$md^{-1}$ (see Tab. 1). Yet, the adaptive significance of active locomotion or buoyancy regulation by more than two thirds of phytoplankton species requires alternative explanation, if not for long-range migration. The largest portion (83%) of modelled $NPP_{\Sigma}$ attributed to migrating phytoplankton is driven by migration speeds ($v$) below 1 $md^{-1}$ (Extended Data Fig. 6). As simulated (and also real) phytoplankton communities regularly comprise fast moving forms such as large dinoflagellates or large diatoms, this means that most contributions derive from slow moving species with $v \approx 0.5$ $md^{-1}$ or less, which is certainly in the capability range of most motile species (Tab. 1). Even modest velocities translate to large vertical distances when microorganisms maintain their direction over the course of days to weeks, either within the lifespan of individual cells or extending over one life cycle at the population level. Long-term up- and down migrations beyond individual cell cycles have previously been proposed for P-uptake in *Trichodesmium*[15]. For sufficiently long unidirectional migrations, autotrophic growth rates of migrators would have to be 0.1–0.3$d^{-1}$ or slower, which is compatible with the considerable fraction of low values within the distribution of measured *in situ* growth rates for the entire phytoplankton community under variable conditions[16,17]. In fact, below a depth of 40m very low growth rates are measured for the dominant fraction of motile and buoyant phytoplankton species[18]. A recent study on SCM in the Mediterranean Sea[19] revealed an average

phytoplankton growth rate of $0.3 d^{-1}$. Such small growth rates are reasonable given prevailing nutrient depletion near the surface and low light availability and temperature in the subsurface near the chemocline. Despite their slow growth rates and the energetic and resource requirements for active migration (e.g. nutrient storage via assimilation into organic forms), migrators (unlike passive drifters) have the competitive advantage of exploiting two essential and spatially separated resources. Their sequential resource uptake could also explain the adaptive significance of the large stoichiometric flexibility in unicellular autotrophs[20,21]. Frequent transitions between high and low nutrient conditions in the picture of up- and down migration makes the ability to regulate nutrient-to-carbon ratios an important trait, which would be a luxury feature in otherwise rather stable oceanic environments.

## S3 Short-range or fast pumping in aquatic environments

Occasional up-migration at high speed has been suggested earlier to act as a nutrient pump from the chemocline towards the surface[13,22]. Long-range up- and downward migrations are known for a relatively limited number of rapidly moving phytoplankton forms: Dinoflagellates, colonies of flagellated cells, and non-flagellated floaters such as cyanobacteria and diatoms that regulate their buoyancy to realize descending and ascending speeds of more than several tens of meters per day[13,23–25]. Observed stoichiometric differences between rapidly sinking and ascending colonies of cyanobacteria constitute some of the best direct evidence for biological nutrient pumping[14]. Carbohydrate ballasting possibly facilitated by carbon over-consumption at high photosynthesis rates may result in the transfer of vacuolated forms to the deep, a physiological mechanism that can be employed by many other autotrophic groups. Short-term (diel) vertical migration of cryptomonads or chlorophyceae is a well studied phosphorus retrieval strategy in lakes[23,26], where distances are typically shorter and gradients steeper than in the ocean.

## S4 Possible consequences of neglecting phytoplankton migration in models

Large-scale spatial patterns of $NPP_{\Sigma}$ predicted by our model differ from satellite-derived estimates, which correlate better with remotely sensed surface fluorescence[2,27], as can be expected from their methodological design. Compared to our approach, they lack stoichiometric plasticity and migration behavior of phytoplankton, effects of nutrient co-limitation, and changes in the nu-

trient supply as described by variable chemocline depths. Satellite-based approaches[27] assume a constant C distribution with depth, which results in NPP profiles that often overrate observations near the surface and underestimate them in the subsurface. In an inter-comparison study, none of 21 examined approaches showed root-mean-squared-deviation in NPP of less than the average NPP for BATS, with similar performance for HOT[4]. Such studies have captured fairly well observed depth integrated $NPP_{\Sigma}$ in the range 500–1000 mg-C$m^{-2}d^{-1}$ but tend to underestimate it by a factor of two where it exceeds 1200 mg-C$m^{-2}d^{-1}$. Though more recent algorithms agree slightly better[2], they still do not reproduce the strong lateral and temporal variability observed by both cruises and station NPP. While satellite-based algorithms predict higher NPP compared to our model in upwelling regions such as off Namibia or Peru and in many coastal zones, they persistently predict lower $NPP_{\Sigma}$ in the vast oligotrophic regions.

Mechanistic biogeochemical (BGC) models as utilized by, e.g., IPCC and CMIP assessments even face greater difficulties reproducing observed production rates and CHL-distributions. When applied at the global scale, their omission of vertically migrating autotrophs results in underestimates of nutrient supply to the surface ocean. In a wide inter-comparison study, most BGC models failed to reach satellite-based estimates of global NPP[28], with two exceptions. By contrast, one model (TOPAZ) displayed significantly higher global NPP than the satellite-based calculations likely because of few extreme model parameter values such as maximum growth rates around $7d^{-1}$ for globally dominant picophytoplankton[29]. Another model (PlankTOM) approached the satellite-based oceanic NPP on average, but underestimated lateral $NPP_{\Sigma}$ gradients, with large mismatches compared to individual campaign data[6].

## S5 Coupling of the PVM model to a 1D physical–biological Eulerian model

We tested the consistency of our sensitivity study on enhanced stratification using an idealized but mechanistic model set-up, where the Lagrangian PVM model was linked to a standard nutrient–phytoplankton–zooplankton–detritus (NPZD) model coupled to the 1D General Ocean Turbulence Model (GOTM)[30,31]. The two latter models were downloaded from the GIT repositories https://github.com/gotm-model and https://github.com/fabm-model/fabm. From the NPZD parametrization, the half-saturation nutrient concentration for phytoplankton growth was changed from 0.3 to 0.1 mmol-N$m^{-3}$ for realizing nutrient depletion in the surface ocean, and the detritus

remineralization rate increased to 0.03 $d^{-1}$ for better activating the microbial loop. The phytoplankton compartment of the model was extended by an imposed concentration of $N_2$ fixers $P_{\mathrm{fix}}$ (in units of nitrogen) in the upper 50m. Furthermore, the concentration $P_{\mathrm{mob}}$ of mobile phytoplankton was added as a normal vertical distribution function around the depth of the chlorophyll maximum ($z_C$) with half width given by the migration amplitude ($\delta z$). Both, $N_2$ fixers and migrating phytoplankton contribute to phytoplankton related processes resolved within the NPZD model such as light shading, mortality (transfer to detritus and the microbial loop), exudation (transfer to dissolved nutrient pool), and grazing. While $N_2$ fixers only act as a nutrient source, migrating phytoplankton were implemented to take up $NO_3$ depending on nutrient availability, hence with highest uptake rates in the chemocline. A coupled simulation of GOTM-$NP_3ZD$ over six years (2010–2015) and time-averaging over the last year resulted in an updated estimate for surface chlorophyll ($CHL_0$) and chemocline depth $z_{\mathrm{N}}$ derived from the simulated nutrient profile (Fig. S6). $CHL_0$ and $z_{\mathrm{N}}$ were in turn passed as input to the PVM model for then updating the values of $P_{\mathrm{mob}}$, $z_C$, and $\delta z$. This sequential coupling of the NPZD and PVM model converged after three to four iterations. Nitrogen-based concentrations were converted to the chlorophyll profiles visualized in Fig. S6 by using the light dependent photoacclimation rule of the PVM model[1].

We adopted a 1D physical GOTM set-up previously developed for the HOT station[32]. A scenario of enhanced stratification was realized by modifying the atmospheric boundary forcing: air temperature was increased by $2^oC$ and wind intensity decreased by 25%. In the NPZD model, the induced decline in upward diffusive nutrient flux led to overall reduced phytoplankton concentration. As we intended to maintain the value of $CHL_0$ (as in the global sensitivity study), $P_{\mathrm{fix}}$ was in the stratification scenario increased by a factor 2.7, which emulated enhanced dominance of $N_2$ fixers.

**Supplementary figures**

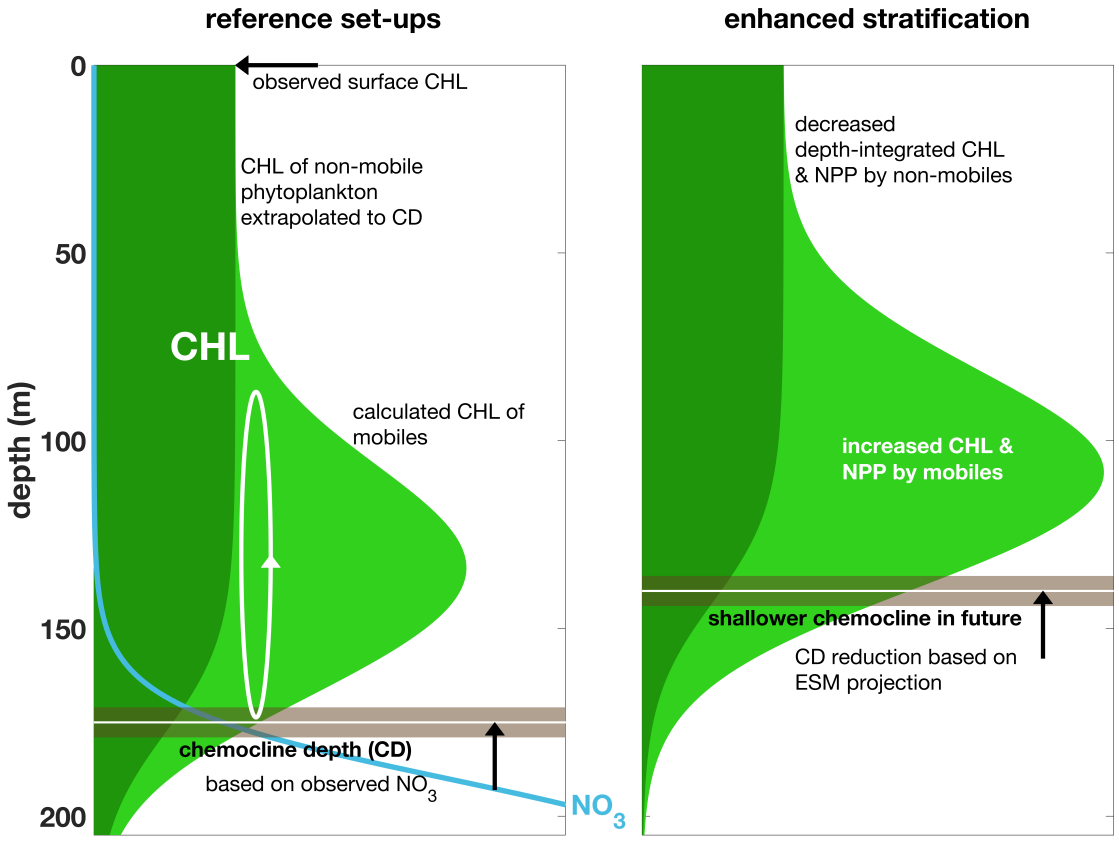


Figure S1: Conceptual design of model set-ups under different nutrient forcings. Left: Reference set-ups of the PVM model. In both the 1D and 3D setup, observed surface chlorophyll ($CHL_0$) is extrapolated up to the chemocline depth $z_N$ for describing the presence of non-mobile phytoplankton (dark green area). Also $z_N$ (brown bar) is based on observations (blue line describing a $NO_3$ profile). The concentration and vertical position of mobile phytoplankton calculated by the PVM model (light green area) adds to the profile of non-mobiles, together determining, e.g., bio-shading of light. The biological pumping of nutrients induced by PVM is assumed to create the observed $NO_3$ profile in combination with other (unknown) sources and sinks such as nutrient uptake by phytoplankton including $N_2$ fixation, nutrient regeneration, or diffusive influx from the chemocline. Right: Climate change sensitivity study with enhanced stratification. The projection of the global MPI-ESM infers local changes, mostly reductions of $z_N$ (Fig. S8), which affect the abundance and positioning of mobile phytoplankton calculated by the PVM model. Their increase compensates for a decline in CHL and NPP by non-mobile phytoplankton, which despite a fixed $CHL_0$ in this sensitivity study originates from the reduced height of the populated water column. The consistency of this scenario is backed up by a simple coupling of the PVM model with a classical physical-biological model that resolves the individual sources and sinks underlaying a change in $z_N$ (Fig. S6).

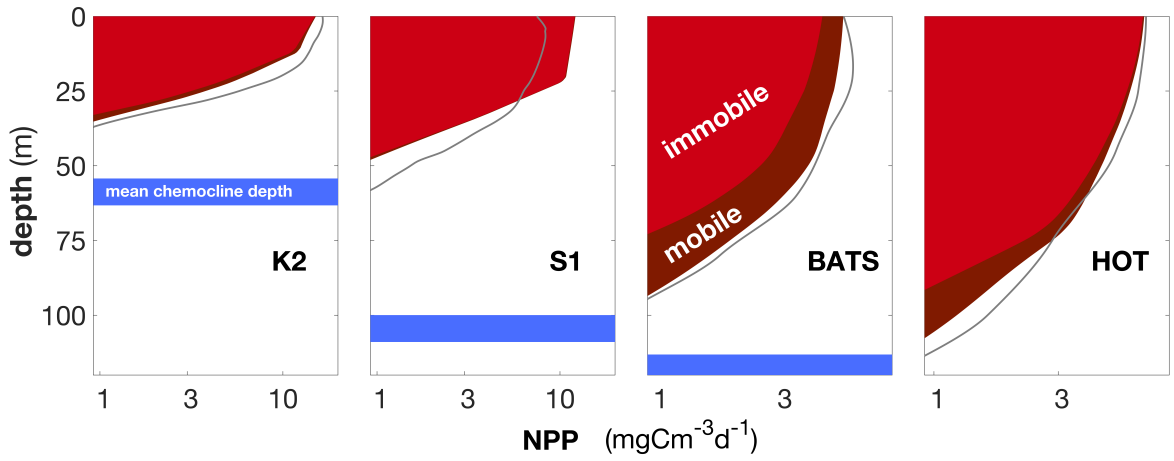


Figure S2: Time-averaged profiles of NPP at four marine time-series stations. Measured (areas) and simulated (grey lines) profiles are displayed for the stations subarctic West Pacific (K2), subtropic West Pacific (S1), Bermuda Atlantic Time-Series (BATS), Hawaii Ocean Time-series (HOT). The contribution of mobile and non-mobile phytoplankton in the simulation is shown as different color shading. Mean chemocline depths $z_N$ are indicated by blue bars. Standard deviations of observed and simulated profiles are given in Extended Data Fig. 1.

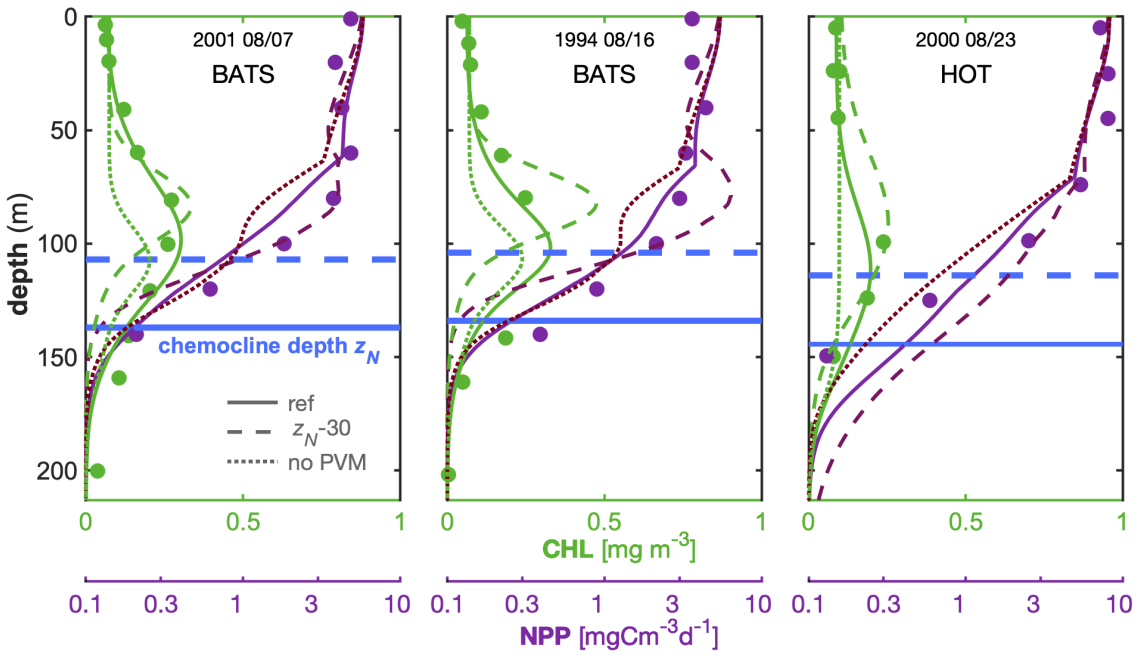


Figure S3: Model sensitivities. The reference run ('ref', solid lines) is compared to a scenario with chemocline depth $z_N$ (blue lines) decreased by 30m (dashed lines) and a model version where PVM is switched off (by restricting migration to 3m and halving the mortality rate to facilitate the build-up of a SCM, dotted lines). At three applications at the stations BATS and HOT were selected according to relatively deep chemoclines. Simulated chlorophyll-a profiles (green lines) and reported data (green circles) are plotted together with measured and simulated NPP profiles (red lines and circles, resp.).

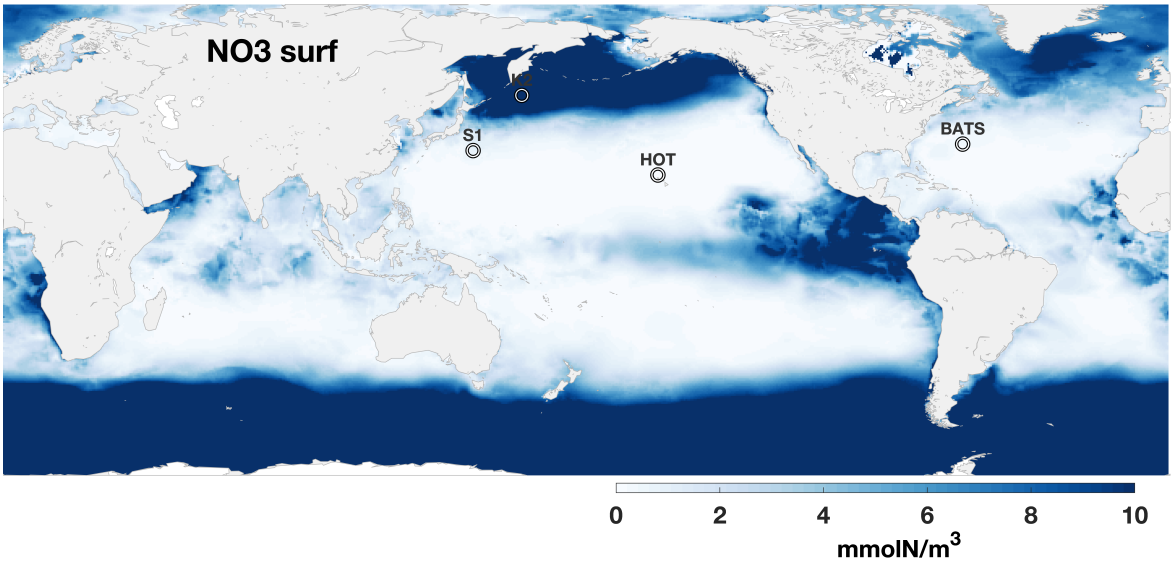


Figure S4: Annual mean of surface nitrate concentration. At a seasonal resolution, the data are used as a proxy for the degree of co-limitation by other nutrients, down-sizing growth and NPP rates, and are based on CARS2009[33,34].

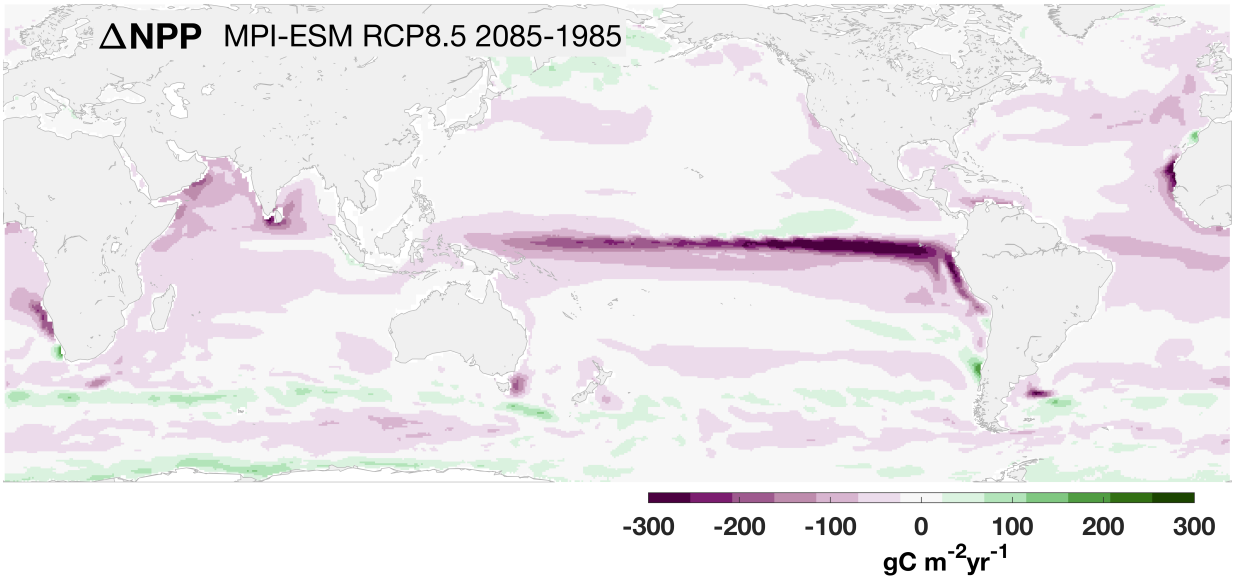


Figure S5: Changes in depth-integrated NPP ($NPP_{\Sigma}$) from the period 1971-2000 to 2071-2100. Here, $NPP_{\Sigma}$ was simulated by the Max-Planck-Institute Earth System Model (MPI-ESM) in a RCP8.5 climate change scenario[35].

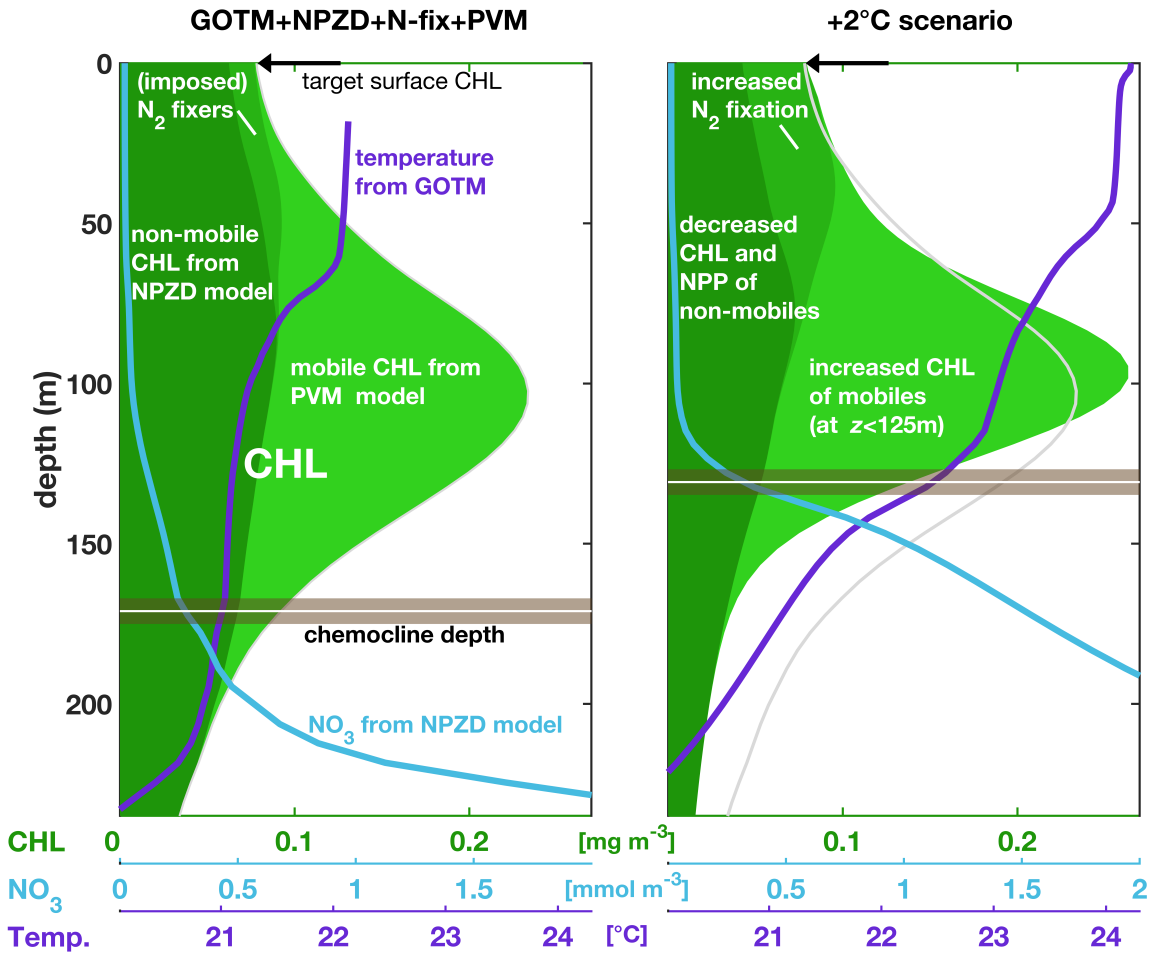


Figure S6: Vertical chlorophyll (CHL) distributions in a coupled Eulerian–Lagrangian model set-up. Left: Profiles of CHL of non-mobile phytoplankton described by an Eulerian NPZD model, $N_2$ fixers (imposed via parameterization), and mobile autotrophs as simulated by the Lagrangian PVM model (green shaded areas). The $NO_3$ profile calculated by the NPZD model (blue line) reflects nutrient uptake by all three phytoplankton groups and their regeneration, but also turbulent diffusive mixing as calculated by GOTM, and allows an estimate of chemocline depth (brown bar). The temperature profile was produced by the underlying GOTM simulation (red line). For details see Sec. S5. Right: Altered atmospheric forcing of GOTM leads to stronger stratification as visible through a steeper vertical temperature gradient. In this Climate Change scenario, the explicit, two-way coupling of the PVM model to the NPZD model produces a new vertical partitioning of the autotrophic community. For comparison, the total CHL concentration of the reference case is shown as grey line.

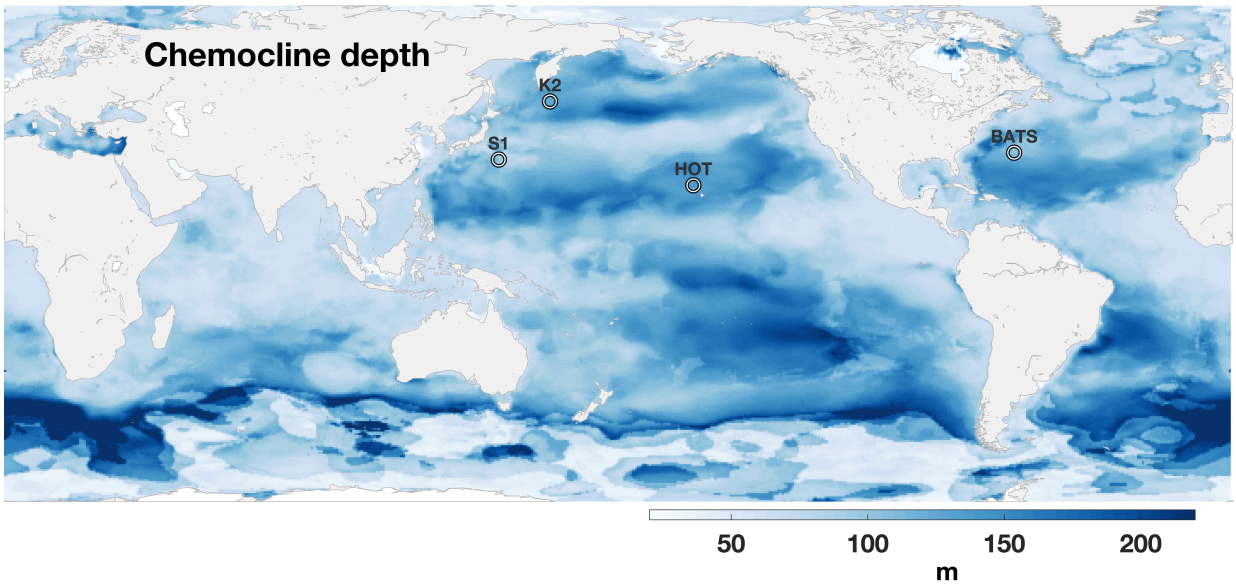


Figure S7: Annual mean of chemocline depth ($z_N$). The global field was calculated using the extrapolated nitrate profile data-set CARS2009.

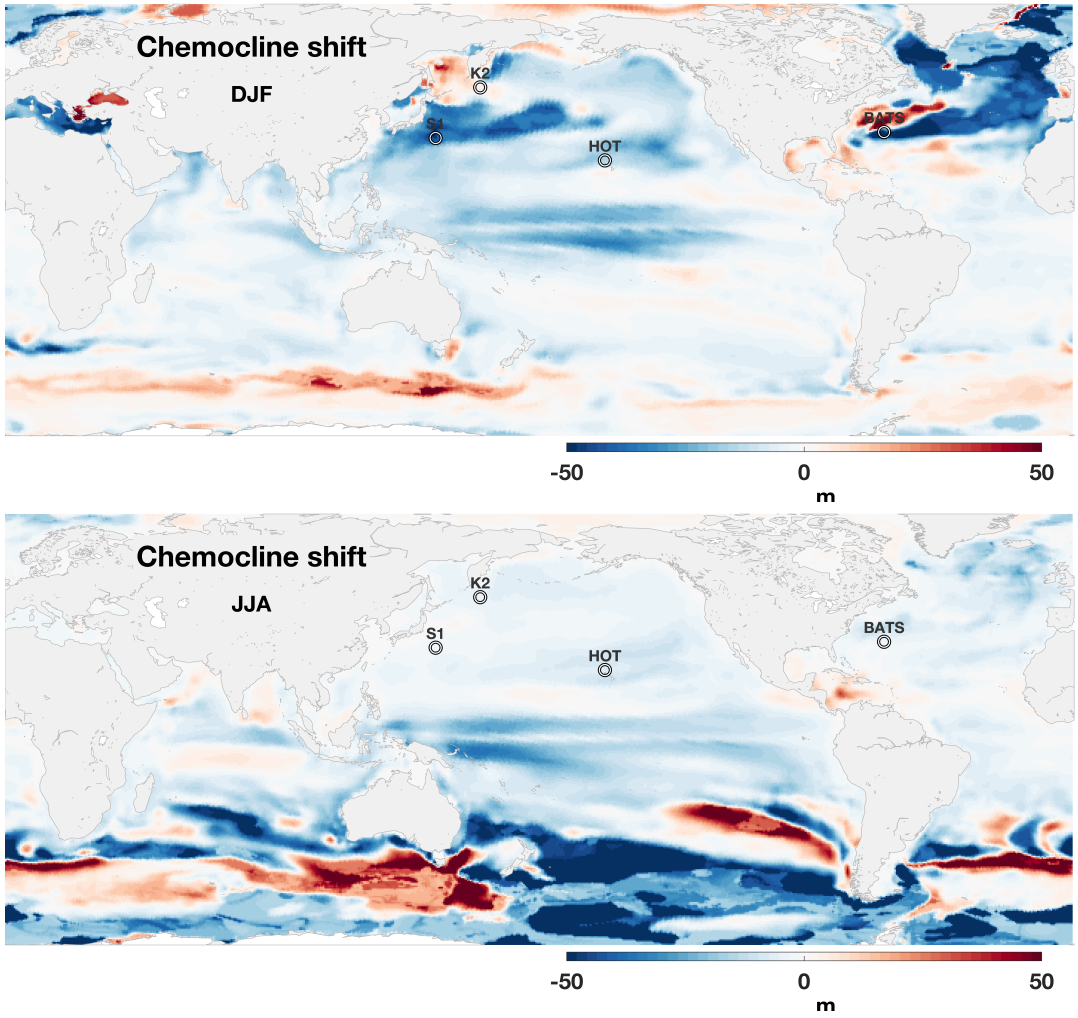


Figure S8: Imposed seasonal shifts in chemocline depth ($z_N$) in a warmer climate. From the four seasons, only winter (DJF) and summer (JJA) are shown. The shifts were estimated from changes in mixed layer depth (MLD) simulated in an RCP8.5 climate change scenario for the time-slice 2071-2100[35]. (For the baseline distibution of $z_N$ see Fig. S7)

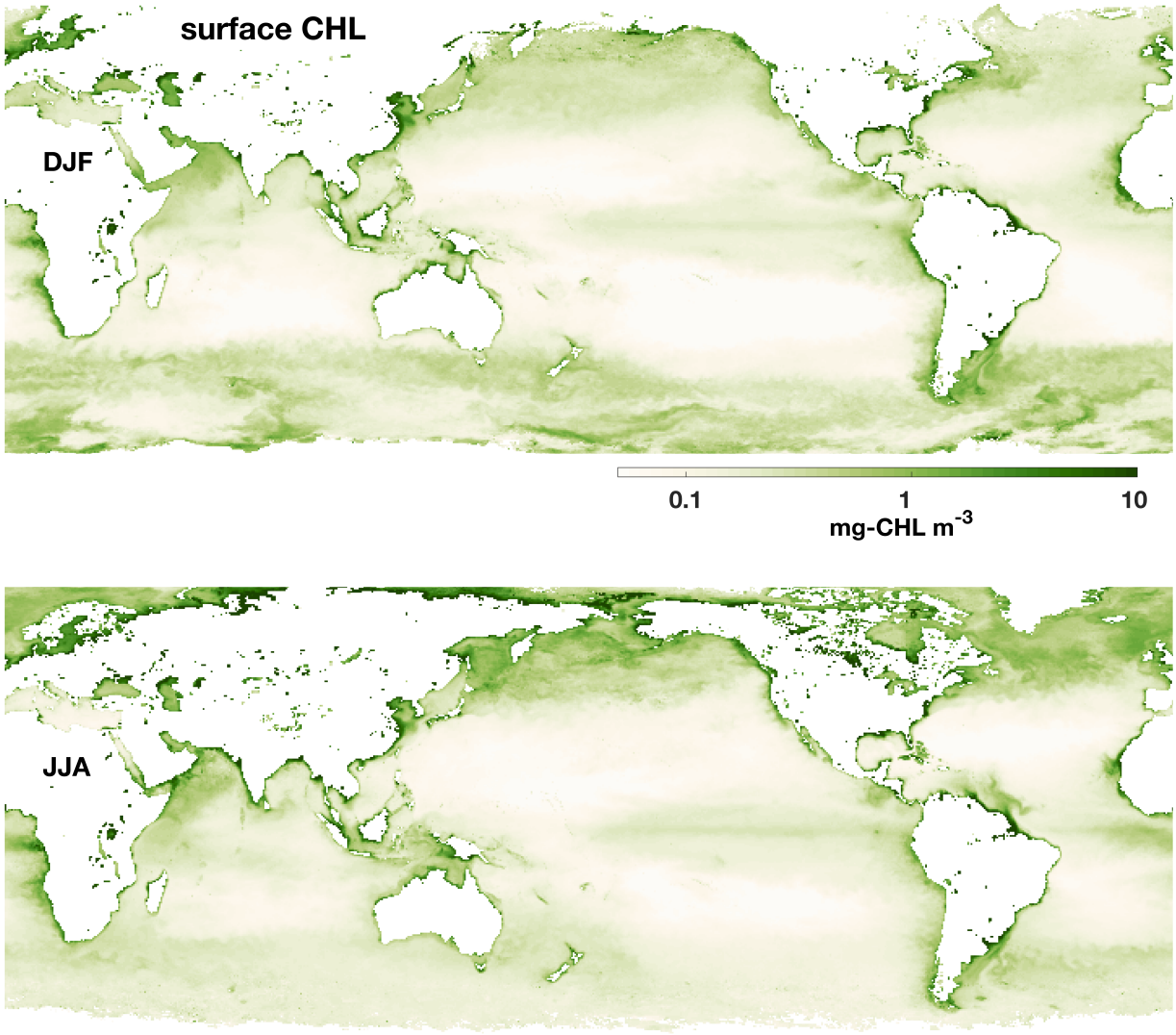


Figure S9: Remotely sensed surface chlorophyll (CHL) from ESACCI v3.1. Data were averaged for winter (December-January-February, upper panel) and summer (June-July-August, lower panel).

## References


1. Wirtz, K. & Smith, S. L. Vertical migration by bulk phytoplankton sustains biodiversity and nutrient input to the surface ocean. *Scientific Reports* **10**, 1142 (2020).

2. Silsbe, G. M., Behrenfeld, M. J., Halsey, K. H., Milligan, A. J. & Westberry, T. K. The CAFE model: A net production model for global ocean phytoplankton. *Glob.Biogeochem. Cycles* **30**, 1756–1777 (2016).

3. Li, Q. P., Wang, Y., Dong, Y. & Gan, J. Modeling long-term change of planktonic ecosystems in the northern South China Sea and the upstream Kuroshio Current. *J. Geophys. Res.* **120**, 3913–3936 (2015).

4. Saba, V. *et al.* An evaluation of ocean color model estimates of marine primary productivity in coastal and pelagic regions across the globe. *Biogeosciences* **8**, 489–503 (2011).

5. Chavez, F. P., Messié, M. & Pennington, J. T. Marine primary production in relation to climate variability and change. *Ann. Rev. Mar. Sci.* **3**, 227–260 (2011).

6. Buitenhuis, E. T., Hashioka, T. & Quéré, C. L. Combined constraints on global ocean primary production using observations and models. *Glob.Biogeochem. Cycles* **27**, 847–858 (2013).

7. Boyd, P. W. *et al.* The decline and fate of an iron-induced subarctic phytoplankton bloom. *Nature* **428**, 549–553 (2004).

8. Fawcett, S. E., Lomas, M. W., Casey, J. R., Ward, B. B. & Sigman, D. M. Assimilation of upwelled nitrate by small eukaryotes in the Sargasso Sea. *Nature Geosci.* **4**, 717–722 (2011).

9. Knapp, A. N., Sigman, D. M. & Lipschultz, F. N isotopic composition of dissolved organic nitrogen and nitrate at the bermuda atlantic time-series study site. *Global Biogeochemical Cycles* **19** (2005).

10. Fawcett, S. E., Ward, B. B., Lomas, M. W. & Sigman, D. M. Vertical decoupling of nitrate assimilation and nitrification in the sargasso sea. *Deep Sea Research Part I* **103**, 64–72 (2015).

11. Gran, H. H. Investigation of the production of plankton outside the Romsdalsfjord 1926-1927. In *Rapport*, vol. 56, 1–112 (Bureau du Conseil permanent international pour l'exploration de la mer, 1929).

12. Hasle, G. R. Phototactic vertical migration in marine dinoflagellates. *Oikos* **2**, 162–175 (1950).

13. Villareal, T. A. *et al.* Upward transport of oceanic nitrate by migrating diatom mats. *Nature* **397**, 423–425 (1999).

14. Villareal, T. & Carpenter, E. Buoyancy regulation and the potential for vertical migration in the oceanic cyanobacterium *Trichodesmium*. *Microb. Ecol.* **45**, 1–10 (2003).

15. Karl, D. M., Letelier, R., Hebel, D. V., Bird, D. F. & Winn, C. D. *Trichodesmium* blooms and new nitrogen in the North Pacific gyre. In *Marine pelagic cyanobacteria: Trichodesmium and other diazotrophs*, 219–237 (Springer, 1992).

16. Furnas, M. J. In situ growth rates of marine phytoplankton: approaches to measurement, community and species growth rates. *J. Plankton Res.* **12**, 1117–1151 (1990).

17. Chen, B. & Liu, H. Relationships between phytoplankton growth and cell size in surface oceans: Interactive effects of temperature, nutrients, and grazing. *Lim. Ocean.* **55**, 965–972 (2010).

18. Furnas, M. J. Net in situ growth rates of phytoplankton in an oligotrophic, tropical shelf ecosystem. *Lim. Ocean.* **36**, 13–29 (1991).

19. Marañón, E. *et al.* Deep maxima of phytoplankton biomass, primary production and bacterial production in the Mediterranean Sea. *Biogeosciences* **18**, 1749–1767 (2021).

20. Klausmeier, C. A., Litchman, E., Daufresne, T. & Levin, S. A. Optimal nitrogen-to-phosphorus stoichiometry of phytoplankton. *Nature* **429**, 171–174 (2004).

21. Wirtz, K. & Kerimoglu, O. Autotrophic stoichiometry emerging from optimality and variable colimitation. *Frontiers Ecol.Evol.* **4**, doi:10.3389/fevo.2016.00131 (2016).

22. Fogg, G. & Walsby, A. Buoyancy regulation and the growth of planktonic blue-green algae. *Int.Verein.Theoret.Angew.Limnol.: Mitt.* **19**, 182–188 (1971).

23. Sommer, U. & Maciej Gliwicz, Z. Long range vertical migration of *Volvox* in tropical Lake Cahora Bassa (Mozambique). *Lim. Ocean.* **31**, 650–653 (1986).

24. Moore, J. K. & Villareal, T. A. Size-ascent rate relationships in positively buoyant marine diatoms. *Lim. Ocean.* **41**, 1514–1520 (1996).

25. Smayda, T. Adaptations and selection of harmful and other dinoflagellate species in upwelling systems. 2. Motility and migratory behaviour. *Progr. Oceanogr.* **85**, 71–91 (2010).

26. Salonen, K., Jones, R. & Arvola, L. Hypolimnetic phosphorus retrieval by diel vertical migrations of lake phytoplankton. *Freshw. Biol.* **14**, 431–438 (1984).

27. Westberry, T., Behrenfeld, M., Siegel, D. & Boss, E. Carbon-based primary productivity modeling with vertically resolved photoacclimation. *Glob.Biogeochem. Cycles* **22** (2008).

28. Laufkötter, C. *et al.* Drivers and uncertainties of future global marine primary production in marine ecosystem models. *Biogeosciences* **12**, 6955–6984 (2015).

29. Dunne, J. P., Gnanadesikan, A., Sarmiento, J. L. & Slater, R. D. Technical description of the prototype version (v0) of tracers of phytoplankton with allometric zooplankton (TOPAZ) ocean biogeochemical model as used in the Princeton IFMIP model. *Biogeosciences* **7**, 3593–3624 (2010).

30. Burchard, H., Deleersnijder, E. & Meister, A. Application of modified patankar schemes to stiff biogeochemical models for the water column. *Ocean Dynamics* **55**, 326–337 (2005).

31. Umlauf, L. & Burchard, H. Second-order turbulence closure models for geophysical boundary layers. a review of recent work. *Cont. Shelf Res.* **25**, 795–827 (2005).

32. Anugerahanti, P., Kerimoglu, O. & Smith, S. L. Enhancing ocean biogeochemical models with phytoplankton variable composition. *Frontiers Mar.Sci.* **8**, 944 (2021).

33. Ridgway, K., Dunn, J. & Wilkin, J. Ocean interpolation by four-dimensional weighted least squares – Application to the waters around Australasia. *J.Atmosph. Ocean.Technol.* **19**, 1357–1375 (2002).

34. CSIRO Atlas of Regional Seas (CARS) (2009). http://www.marine.csiro.au/ dunn/cars2009.

35. Giorgetta, M. A. *et al.* Climate and carbon cycle changes from 1850 to 2100 in MPI-ESM simulations for the Coupled Model Intercomparison Project phase 5. *J. Adv. Mod. Earth Sys.* **5**, 572–597 (2013).